4176–4187 *Nucleic Acids Research, 2018, Vol. 46, No. 8* *Published online 5 February 2018*
doi: 10.1093/nar/gky071

Translation initiation of alphavirus mRNA reveals new insights into the topology of the 48S initiation complex

René Toribio[1], Irene Díaz-López[1], Jasminka Boskovic[2] and Iván Ventoso[1,*]

[1]Centro de Biología Molecular 'Severo Ochoa' (CSIC-UAM), Departamento de Biología Molecular, Universidad Autónoma de Madrid (UAM), 28049 Madrid, Spain and [2]Structural Biology Programme, Electron Microscopy Unit, Spanish National Cancer Research Center (CNIO), 28029 Madrid, Spain

Received June 22, 2017; Revised January 22, 2018; Editorial Decision January 23, 2018; Accepted February 01, 2018

ABSTRACT

The topology and dynamics of the scanning ribosomal 43S pre-initiation complex (PIC) bound to mRNA and initiation factors (eIFs) are probably the least understood aspects of translation initiation in eukaryotes. Recently, we described a trapping mechanism in alphavirus that stalls the PIC during scanning of viral mRNA. Using this model, we were able to snapshot for the first time the eIF4A helicase bound to mRNA in a 48S initiation complex assembled *in vitro*. This interaction was only detected in the presence of the natural stem loop structure (DLP) located downstream from the AUG in viral mRNA that promoted stalling of the PIC, suggesting that DLP stability was enough to jam the helicase activity of eIF4A in a fraction of assembled 48S complexes. However, a substantial proportion of DLP mRNA molecules were effectively unwound by eIF4A *in vitro*, an activity that alphaviruses counteract in infected cells by excluding eIF4A from viral factories. Our data indicated that eIF4A–mRNA contact occurred in (or near) the ES6S region of the 40S subunit, suggesting that incoming mRNA sequences penetrate through the ES6S region during the scanning process. We propose a topological model of the scanning PIC and how some viruses have exploited this topology to translate their mRNAs with fewer eIF requirements.

INTRODUCTION

Translation initiation in eukaryotes is a multistep process that involves activation of the mRNA, attachment of the ribosomal pre-initiation complex (43S PIC), and for most mRNAs, 3′ movement ('scanning') of the PIC to locate the initiation codon (48S complex formation), necessary for 60S subunit binding (1). This process is assisted by a set of initiation factors (eIFs) that work cooperatively through a coordinated chain of interactions. The eIF4F complex (eIF4E+4A+4G) is mainly involved in mRNA activation, attachment and scanning, whereas eIF2 bound to Met-tRNA and GTP (ternary complex), eIF5, eIF1 and eIF1A are mainly involved in recognition of the initiation codon. eIF3, a multiprotein complex that encircles 40S, is involved in almost every step of translation initiation (2–4). The proportion of PICs that reach the initiation codon is variable, directly related to the complexity of secondary structures in the 5′-UTR of mRNA that must be removed (5–9). Scanning of the 43S PIC requires the participation of RNA helicases that convert the incoming RNA into a single-stranded form for proper codon inspection in the decoding groove of 40S (10). eIF4A is the canonical RNA helicase, that associates with eIF4E and eIF4G to bind near the 5′ end of mRNA, promoting 43S loading and the subsequent scanning process (11–14). Helicase activity of eIF4A is highly stimulated by eIF4G binding that clamps the two domains of eIF4A, thus increasing the affinity for RNA and adenosine triphosphate (ATP) (15). It is thought that eIF4A promotes unidirectional (toward 3′) scanning of the 43S complex by alternating cycles of binding and dissociation from mRNA in an ATP-dependent manner, and although the topology of PIC scanning has not been determined yet, two models have been proposed. In the first model, the eIF4F complex is placed ahead of the 43S PIC, unwinding incoming RNA structures while pulling the complex toward the 3′ end (15). In the second model, eIF4A acts as a simple RNA clamp at the trailing edge, pushing the 43S PIC (16). Mapping the exact placement of eIF4F within the scanning PIC should definitely clarify this issue, though the presumably dynamic nature of 43S/mRNA/eIF4F interactions has severely limited the ability of cryo-EM techniques to reconstruct the whole 48S initiation complex (17–20). Moreover, no stable interaction has been detected between eIF4A and mRNA sequences within the 48S complex.

The study of alphavirus (Sindbis (SV) and Semliki Forest (SFV)) mRNA translation has recently revealed how the secondary structure (DLP) located 25–37 nt downstream from the AUG of viral 26S mRNA can influence recogni-

*To whom correspondence should be addressed. Tel: +34 911 964 809; Fax: +34 911 964 420; Email: iventoso@cbm.csic.es
Present address: René Toribio, Centro de Biotecnología y Genómica de Plantas, UPM-INIA, Madrid, Spain.

© The Author(s) 2018. Published by Oxford University Press on behalf of Nucleic Acids Research.
This is an Open Access article distributed under the terms of the Creative Commons Attribution License (http://creativecommons.org/licenses/by-nc/4.0/), which permits non-commercial re-use, distribution, and reproduction in any medium, provided the original work is properly cited. For commercial re-use, please contact journals.permissions@oup.com

Downloaded from https://academic.oup.com/nar/article-abstract/46/8/4176/4838059 by Spanish National Cancer Research Center user on 23 October 2018

tion of the initiation codon, stalling advance of the scanning PIC by interacting with the ES6S region of the 40S subunit (21,22). This RNA trapping mechanism has been interpreted as an adaptation of these viruses to enable translation initiation even when eIF2 becomes inactivated by protein kinase R in vertebrate hosts (23,24). Under these circumstances, it is not clear how the Met-tRNAi can be transferred to the initiation complex of viral 26S mRNA. The participation of alternative eIFs as eIF2A, eIF2D and eIF5B has been suggested, although the possibility that Met-tRNAi could enter the complex by simple diffusion, perhaps with the help of some viral product(s), is still open (24–26). In this work, we used this feature of alphavirus mRNA to snapshot the scanning complex *in vitro*, which allowed us to detect the contacts of eIF4A with mRNA in ES6S region of 40S subunit.

MATERIALS AND METHODS

Synthesis of mRNA

Minimal versions of SV and SFV mRNAs with U residues at defined positions were synthesized *in vitro* by T7 RNA polymerase (NEB) in the presence of 4-thio-UTP (4-thio-U) as described recently (21). The transcription mixture also included 30 μCi [α-^{32}P]GTP, and the resulting mRNAs were purified through Chromaspin-30 columns (Clontech). Condensed versions of SV 26S mRNA encoding only capsid protein but with the 5′ and 3′ UTRs from natural 26S mRNA were prepared (SV DLP-capsid and SV ΔDLP-capsid). These mRNAs were synthesized using transcription and capping kits from NEB (HiScribe T7 Quick, Vaccinia capping system).

Recombinant viruses and infection

SV-eIF4A virus was constructed by cloning the human eIF4AI gene into the pTE/5′2J infectious clone, such that the heterologous gene is transcribed from a second subgenomic promotor (21). The primers used were: forward AGTAGCGGCCGCATGTCTGCGA GCCAGGATTCCCG; reverse CCGCGGGGCCCTCA CAGATCCTCTTCTGAGATGA GTTTTTGTTCGA TGAGGTCAGCAACATTGAGGGGC. The resulting polymerase chain reaction product was cloned into the pTE/5′2J-EGFP plasmid (21) using NotI and ApaI, such that the EGFP gene was replaced with eIF4AI. We also included the SFV DLP structure downstream from the AUG of heterologous mRNA to improve its translation in infected cells. Plasmids were linearized with XhoI enzyme and transcribed *in vitro* with SP6 RNA polymerase (NEB) in the presence of a cap analog (^{7}methyl-GTP, Promega), which typically generates mRNAs that are 50–60% capped. About 3 μg of *in vitro*-synthesized SV RNA was electroporated into ∼10^{7} BHK21 cells, and virus was recovered after cytopathic effect was complete. Recombinant viruses were further amplified in BHK21 cells and purified on a sucrose cushion as described previously (21). For virus infections, mouse BHK21 and 3T3 cells were infected with the indicated viruses at a multiplicity of infection (MOI) of 25 pfu/cell in 24-well plates and analyzed at 5–6 hpi.

UV crosslinking experiments

Crosslinking experiments using [^{32}P]-labeled mRNAs with photoreactive 4-thio-U were carried out as described recently (21). After crosslinking, lysates were centrifuged over a 20% sucrose cushion at 90 000 × *g* for 3 h, and the whole ribosomal fraction (WRF) was resuspended in 50 μl of TE buffer. For 48S isolation, lysates were centrifuged on a 10–35% sucrose gradient at 45 000 rpm for 3 h in an SW50.1 rotor. For protein analysis, samples were digested with RNAse A and T1 for 1 h at 37°C before sodium dodecyl sulphate-polyacrylamide gel electrophoresis (SDS-PAGE) analysis. For RNA analysis of crosslinking products, samples were digested with proteinase K and RNA was extracted twice with phenol and then precipitated in ethanol. RNase H assays were carried out as described previously (21). Briefly, samples were annealed at 65°C for 5′ with 10 pmol of oligonucleotides covering the indicated regions of 18S rRNA and digested with 5 U of RNase H (NEB) for 15 min at 37°C. Finally, the samples were analyzed by denaturing agarose gel electrophoresis, transferred to nitrocellulose membrane and exposed to X-ray films.

Denaturing immunoprecipitation

The ribosomal fraction from a 500 μl translation reaction including 2 μg of [α-^{32}P]-4-thio-U- SV-DLP U1 mRNA and GMP-PNP was obtained as described above and denatured in a buffer containing Tris–HCl 50 mM pH 7.4, 5 mM EDTA, 10 mM dithiothreitol (DTT) and 5% w/v SDS as described previously (27). After 5 min boiling, samples were kept on ice and slowly renatured by 10-fold dilution in Tris-HCl 50 mM pH 7.4, 150 mM NaCl, 5 mM ethylenediaminetetraacetic acid (EDTA) and 1% Triton X-100. Then, the extract was divided in two parts, incubated either with α-eIF4A antisera (St John's lab, STJ27247) or α-RPS6 (St Cruz) O/N at 4°C. Next, a mixture of protein A/G conjugated to magnetic beads (Thermo Fisher Scientific) was added and incubated for an extra hour at RT, and immunoprecipitated complexes were analyzed by SDS-PAGE and autoradiography.

Toeprinting assays

Toeprinting analysis was carried out essentially as described previously (28). Each 10-μl reaction contained 7.5 μl of rabbit reticulocyte lysates (RRL) (Promega) and either 2 mM of GMP-PNP (for 48S assembly) or 0.8 μg/μl of cycloheximide (for 80S assembly), with the final magnesium acetate concentration adjusted to 2.5 and 1 mM, respectively. Lysates were pre-incubated for 10 min at 30°C, and 150 ng of capped mRNAs were added and incubated for an additional 20 min at 30°C. Then, an equal volume of RT mix containing 0.5 mM dNTP mix, 1× RT buffer, 5 mM DTT, 10 pmol VIC-labeled capsid primer (24) and 200 U of SuperScript™ III RT enzyme (Invitrogen) were added and samples were incubated at 37°C for 40 min. At this temperature, we found that RT proceeded through the DLP structure without any extension arrest. Finally, samples were extracted twice with phenol/chloroform/IAA, ethanol precipitated and analyzed in a 3130XL Genetic Analyzer (Applied Biosystems).

Downloaded from https://academic.oup.com/nar/article-abstract/46/8/4176/4838059 by Spanish National Cancer Research Center user on 23 October 2018

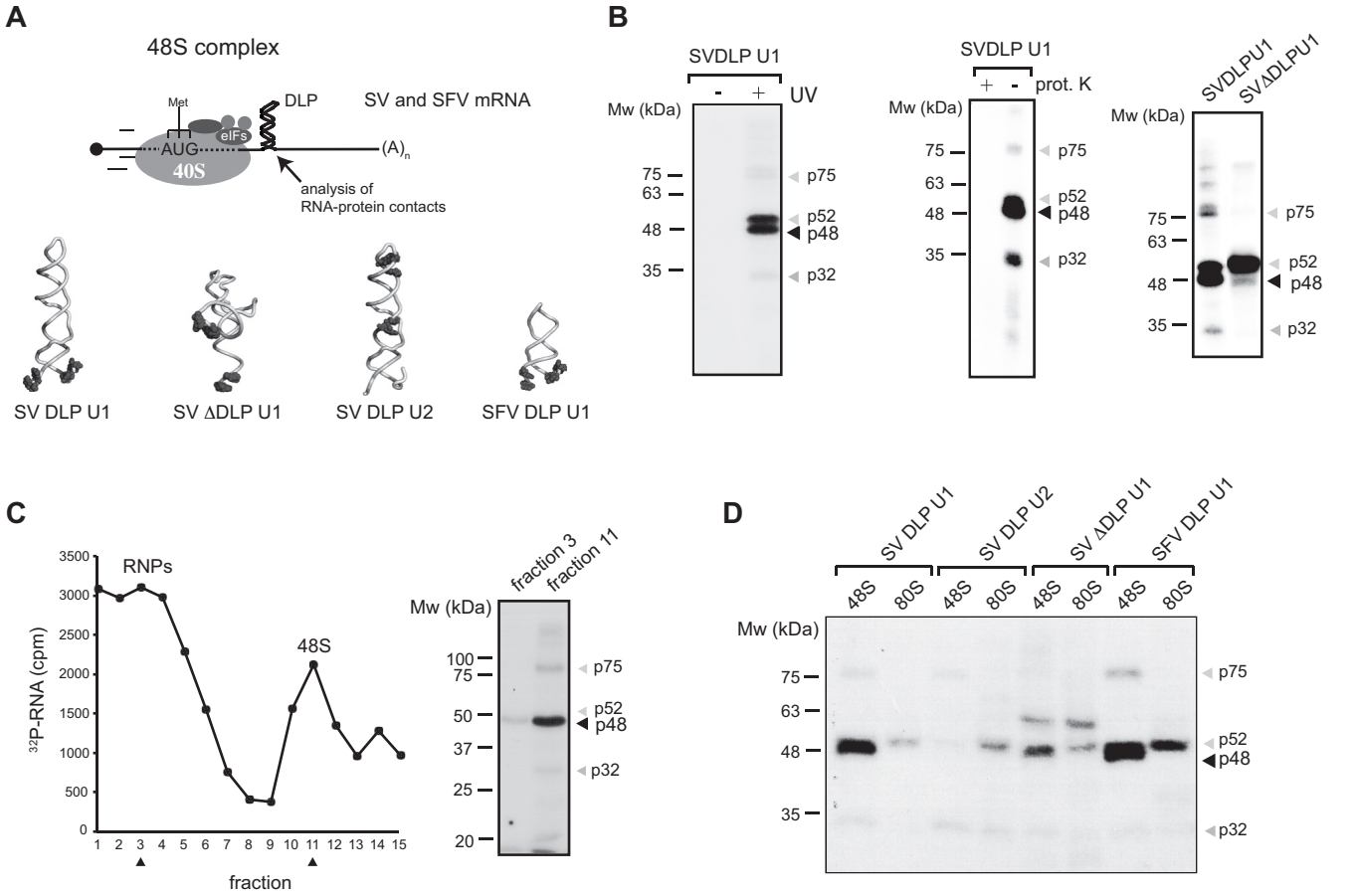

Figure 1. Analysis of proteins crosslinked to DLP mRNA in 48S complexes assembled in RRL. (**A**) Schematic diagram of the assembled 48S complex on mRNA showing a DLP structure located at 28 (SV) and 31 (SFV) nt downstream from the AUG. Four different mRNAs were used, containing 4-thio-U residues at the indicated positions (black dots). (**B**) Crosslinking of [^{32}P]-labeled SV-DLPU1 mRNA with proteins of the 48S complex analyzed from crude ribosomal fraction (P100). Where indicated, the lysates were irradiated or not with UV (right panel), and treated or not with 10 μg of proteinase K for 30 min before analysis (middle panel). The right panel shows a crosslinking experiment programmed with SV-DLP U1 or SV-ΔDLP U1 mRNAs. In all cases, samples were extensively digested with RNAses and analyzed by SDS-PAGE followed by autoradiography as described in 'Materials and Methods' section. (**C**) Crosslinking of [^{32}P]-labeled SV-DLPU1 mRNA in 48S complexes isolated by sucrose gradient centrifugation. The fractions analyzed are marked with arrowheads. (**D**) Crosslinking patterns using the indicated mRNAs in the 48S complex (by GMP-PNP) or in the 80S complex (by cycloheximide). Note that the p48 band was only detected in 48S complexes assembled with DLP-containing mRNA, bearing 4-thio-U at the base of DLP structure.

Probing and modeling RNA structures

SHAPE (selective 2′-hydroxyl acylation and primer extension) was used for probing RNA structure with N-methylisatoic anhydride (NMIA) that reacts with unpaired nucleotides of RNA (29). Approximately 5 pmol of RNA was treated with 5–16 mM NMIA (Invitrogen) for 45 min at 37°C, precipitated with isopropanol and retrotranscribed with Superscript III (Invitrogen) using 5′-labeled [γ−^{32}P] DLP′s-3′ primer. In parallel, RNA was retrotranscribed with 1 mM ddNTPs/1 mM dNTPs for sequencing. Fragments were analyzed in 10% acrylamide-urea gels and bands were quantified by densitometry and normalized. SHAPE data were used as constraints to generate 2D and 3D models using the MC-fold and RNAComposer pipelines (21). RNAfold (Vienna RNA Web Services) was routinely used to calculate the minimal folding energy of centroid RNA structures and base pair probabilities.

In vitro translation

In vitro translation was performed in nuclease-treated RRL (Promega) using 150 ng of capped SV DLP-capsid or SV ΔDLP-capsid mRNAs in the presence of 15 μCi of [^{35}S]-Met for 60 min at 30°C. Samples were denatured in sample buffer and analyzed by SDS-PAGE and autoradiography as described previously (24).

Western blot and immunofluorescence

Western blots were carried out as described previously (24) using the following primary antibodies: α-myc (Clontech), α-SV E1, α-SV C, α-eIF2 (Santa Cruz Biotech.), α-RPS7 (Santa Cruz Biotech.), α-RPS2 (Santa Cruz Biotech.), α-RPS6 (Santa Cruz Biotech.), mouse α-eIF4A (a gift of M. Altmann, University of Bern, Switzerland) and rabbit α-eIF4A (St John's lab, STJ27247). Blots were developed with ECL (GE) and bands were quantified by densitometry. Immunofluorescence (IF) analysis was carried out as described previously using α-SV C (1:500), α-SFV C (1:500)

Downloaded from https://academic.oup.com/nar/article-abstract/46/8/4176/4838059 by Spanish National Cancer Research Center user on 23 October 2018

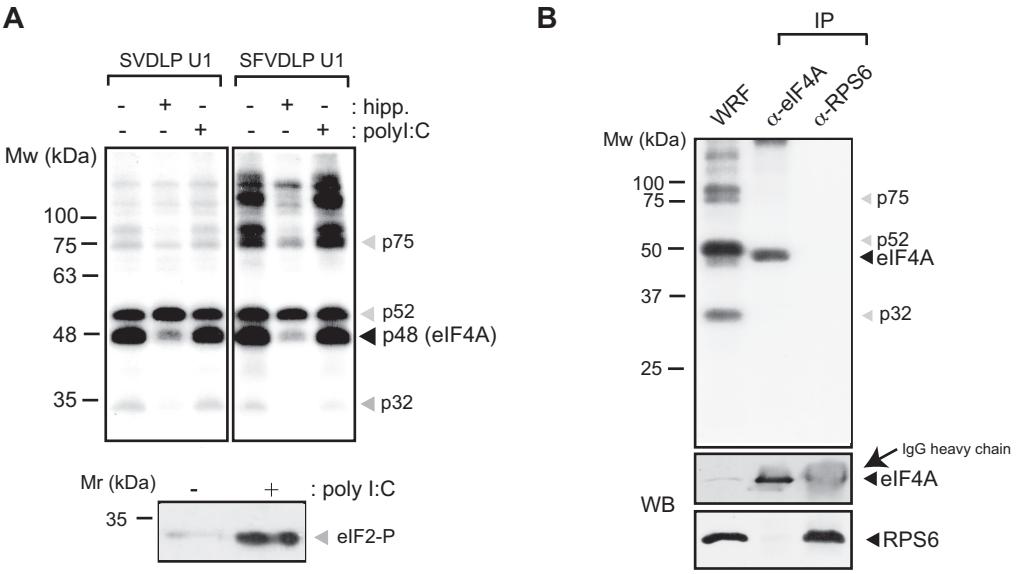

Figure 2. eIF4A interacts with the base of the DLP RNA in the 48S complex. (**A**) Crosslinking assays using SV-DLP U1 and SFV-DLP U1 mRNAs in the presence of hippuristanol or polyI:C. Samples were treated with 1 μM of hippuristanol or 0.5 ng/μl poly I:C to block eIF4A or to induce eIF2α phosphorylation, respectively, as indicated. Then, P100 fractions were obtained and equivalent cpms were analyzed by SDS-PAGE and autoradiography. The lower panel shows typical eIF2α phosphorylation induced by poly I:C treatment of RRL. (**B**) Denaturing IP with anti-eIF4A and anti-RPS6 antibodies. 48S complexes were assembled with SV-DLP U1 mRNA, crosslinked and the WRF was denatured and subjected to IP with the indicated antibodies (as described in 'Materials and Methods' section).

and mouse α-eIF4A (1:20) as primary antibodies, and α-mouse Alexa 488 or α-rabbit Alexa 595 as secondary antibodies (Invitrogen). The preparations were analyzed in a Zeiss Axioskop 2 plus fluorescence microscope.

Immunoelectron microscopy

To locate eIF4A in the 48S complex, 300 μl of RRL were incubated with 0.2 and 3 μg of fluorescein-labeled and unlabeled SV-DLP U1 mRNA, respectively, and 48S complexes were allowed to assemble in the presence of GMP-PNP as described above. Then, lysates were fixed on ice with 1% formaldehyde for 20 min and quenched with 0.3 M glycine and Tris–HCl 50 mM pH 7.5. The lysates were centrifuged in a 10–35% sucrose gradient for 2.5 h at 40 000 rpm in a Beckman SW50 rotor and fractionated from the bottom. The peak 48S fraction was identified by measuring the fluorescence of fractions incubated with 1:25 α-eIF4A (St John's lab, STJ27247) antibody for 3 h at 4°C. Then, ribosomal complexes were sedimented at 90 000 rpm for 90 min in a TLA100.1 rotor, resuspended in 50 μl of polysome buffer and incubated for 90 min at 4°C with a 1:100 dilution of 5 nm colloidal gold-labeled protein A (GPA, University Medical Center Utrecht). To locate mRNA region downstream of AUG within the 48S complex, we used SV ΔDLP U1 mRNA bound to a 5′-biotinylated RNA oligo (AAGGUA AUGGUCGUCGUCCG) that hybridizes in the region 25–45 nt of the mRNA coding sequence (CDS). Finally, samples were negatively stained for electron microscopy analysis. The samples were visualized in a Tecnai 12 transmission EM (FEI, Netherlands) or in a Jeol 1230 operating at 120 and 100 keV, respectively. Images were recorded on a TVIPS CMOS camera at 61 320 × nominal magnification (2.5 Å/pixel). Only labeled particles whose orientation were unambiguously determined by two-axis measurement were selected and grouped into similarity classes.

RESULTS

Crosslinking of eIF4A and mRNA within the 48S complex

We recently used minimal versions of SV and SFV 26S mRNAs labeled with photoreactive 4-thio-U residues to detect the interaction of the DLP with the solvent side of 48S complex (21). Analysis of RNA–RNA crosslinking revealed specific contacts between the DLP base (SV and SFV U1 mRNAs) and regions of 18S rRNA located on the solvent side, including the ES6S and h16–18 helices (21). In order to extend to other components of 48S complex, we analyzed protein crosslinking with [^{32}P]-SV mRNA U1 in the presence of GMP-PNP, a non-hydrolyzable GTP analog that freezes 48S PIC upon initiation codon recognition (late stage initiation complex) (Figure 1A). Proteins that are contacting SV and SFV mRNAs within initiation complex can be crosslinked to photoreactive 4-thio-U residues placed at the indicated positions in the mRNAs, and then analyzed upon extensive digestion of complexes with RNAses. 48S complexes were assembled in RRL and analyzed directly from the ribosomal P100 fraction (Figure 1B), or further separated by centrifugation in sucrose gradients (Figure 1C). SDS-PAGE analysis revealed at least two prominent protein bands in the range of 48–50 kDa, that crosslinked with the DLP base of 48S, and two additional fainter bands of 32 and 75 kDa whose intensity varied among RRL batches (Figure 1B). SV and SFV mRNAs generated a similar pattern of protein crosslinking, whereas neither p48 nor p32 bands were detected when a mutated mRNA lacking the DLP structure was used (Fig-

Downloaded from https://academic.oup.com/nar/article-abstract/46/8/4176/4838059 by Spanish National Cancer Research Center user on 23 October 2018

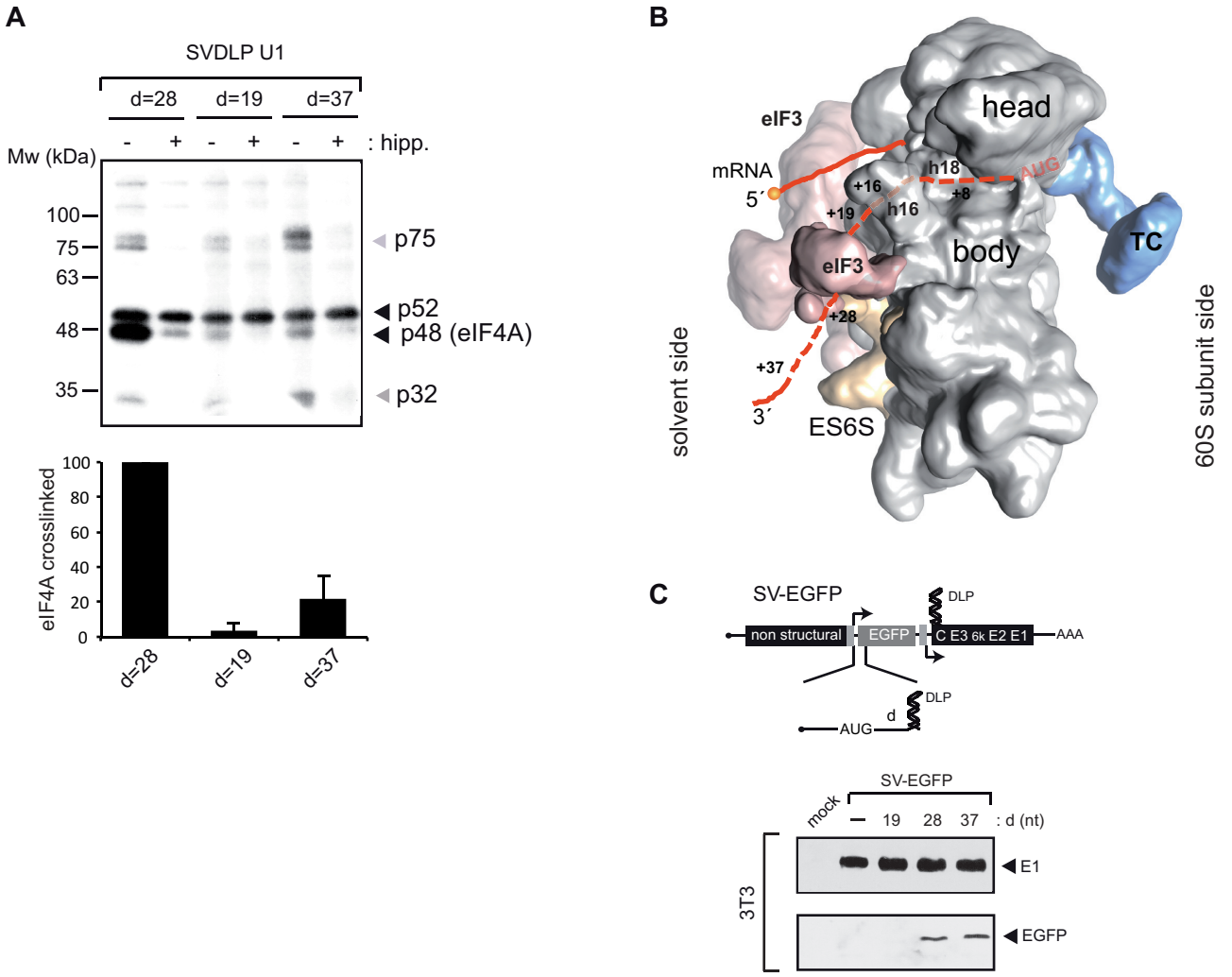

Figure 3. eIF4A crosslinking with SV mRNA is DLP position dependent. (**A**) Variants of SV-DLP U1 mRNA where the distance from the AUG was shortened ($d = 19$) or extended ($d = 37$) were used. Quantification of eIF4A crosslinking from three independent experiments (mean ± SEM) is shown in the bottom panel. (**B**) Model of 43S complex bound to mRNA showing the approximate positions of DLP structures at $d = 19$, 28 and 37, assuming that mRNA penetrates through the $ES6S^A$ and $ES6S^B$ helices of the 40S subunit. The positions of eIF3 and the ternary complex (TC) are also shown. (**C**) Translation activity of DLP structures located 19, 28 and 37 nt from the AUG. Recombinant virus expressing an EGFP reporter mRNA (SV-EGFP) bearing the DLP structure located at the indicated position (d) or lacking it (−) were obtained and described previously (21). 3T3 cells were infected with the indicated viruses at an MOI of 10, extracts were made at 6 hpi and analyzed by western blot with the indicated antibodies.

ure 1B). Moreover, no crosslinking of p48 was detected when 4-thio-U was placed in the middle and apical region of DLP structure (SV DLP U2 mRNA), showing that this protein contacted only the nucleotides flanking the base of the DLP (Figure 1D). We next compared the patterns of protein crosslinking in 48S and 80S complexes by using cycloheximide instead of GMP-PNP to block the 80S initiation complex at the pre-translocation step (30). As shown in Figure 1D, the p48 band was not detected in 80S complexes assembled with SV or SFV U1 mRNAs, whereas p52 was even enriched in the 80S complex in some cases. The size and behavior of the 48 kDa band (p48) resembled eIF4A, the main RNA helicase of 48S complex that associates with eIF4G (11). To verify this, we first used hippuristanol, a potent and highly specific inhibitor of the RNA binding and helicase activities of eIF4A (31). Addition of hippuristanol to translation mixtures decreased the intensity of the 48 kDa band in a specific manner (Figure 2A), confirming that it was indeed eIF4A. To further confirm this point, we carried out denaturing immunoprecipitation (IP) of crosslinked lysates using an anti-eIF4A antibody. Before IP, the lysates were denatured by SDS treatment to prevent accidental co-precipitation of associated proteins. As shown in Figure 2B, the 48 kDa band was specifically immunoprecipitated by anti-eIF4A antibodies.

We next carried out similar experiments using β-globin mRNA to assemble the 48S complex. β-globin mRNA lacks a DLP-like structure, but it contains only a single adenine in the 27–51 region of the CDS, which allowed us to design an RNA probe lacking internal uracils. Once annealed to the β-globin mRNA, this probe mimicked the stem part of the SV DLP RNA structure and had comparable stability (Supplementary Figure S1A). It also contained two unpaired, photoreactive 4-thio-U residues at the 3′ end so

Downloaded from https://academic.oup.com/nar/article-abstract/46/8/4176/4838059 by Spanish National Cancer Research Center user on 23 October 2018

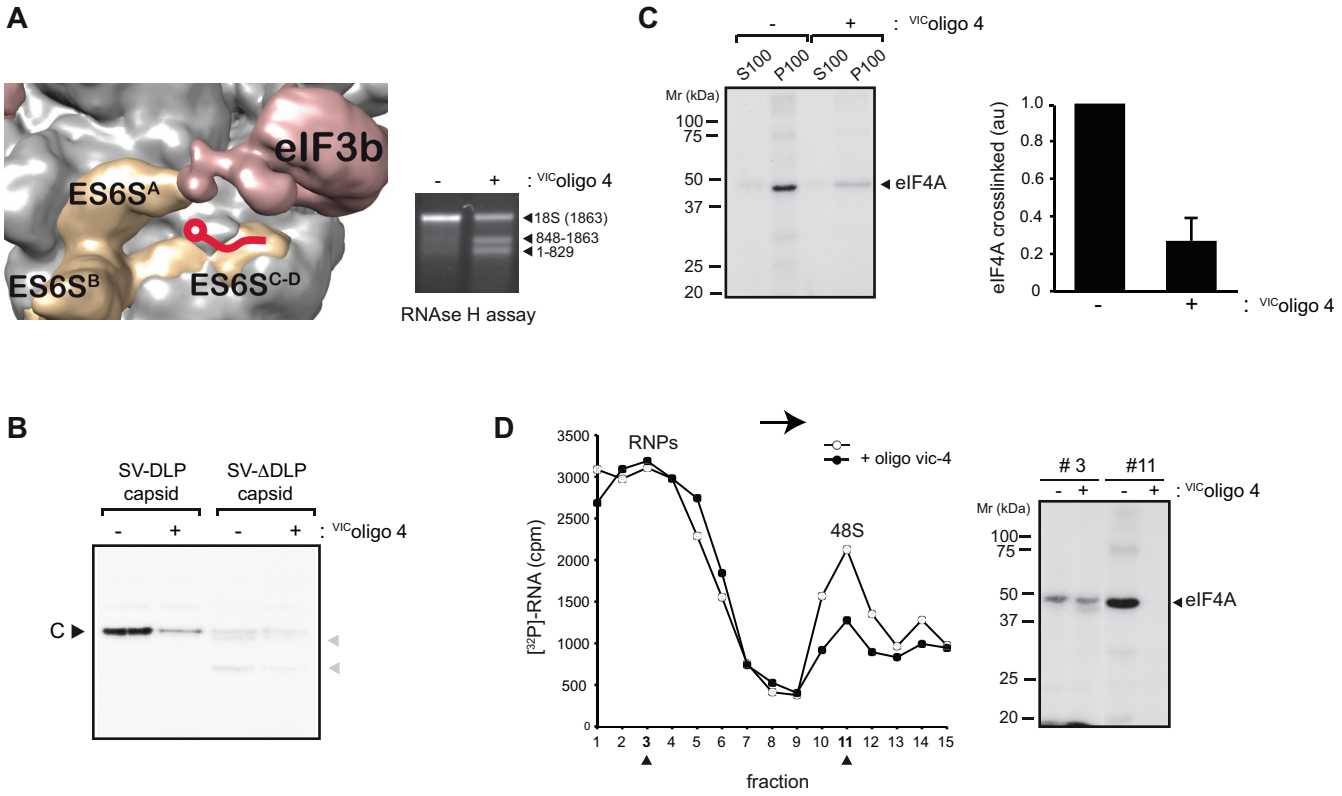

Figure 4. Effect of ^{VIC}oligo-4 on the interaction of eIF4A in the 48S complex with the base of the DLP structure. (**A**) 43S model showing the binding site of ^{VIC}oligo-4 to the ES6S^{C-D} helix. ^{VIC}oligo-4 binding to purified rabbit 40S subunit was analyzed by RNAse H cleavage as described previously (21). The resulting 18S rRNA fragments were analyzed by electrophoresis in a 0.8% agarose gel. (**B**) Effect of ^{VIC}oligo-4 addition (10 μM) on translation programmed with SV DLP capsid and SV ΔDLP capsid mRNAs in RRL. Note that elimination of the DLP structure impaired AUG recognition, giving rise to aberrant products (gray arrowheads) that resulted from spurious initiation at downstream AUGs, as reported previously (24). (**C**) Crosslinking assays using SV DLPU1 mRNA in the presence of 10 μM of ^{VIC}oligo-4. Ribosomal fractions (P100) and post-ribosomal fractions (S100) were analyzed. The change in intensity of the eIF4A band was measured from three independent experiments; data are represented as the mean ± SEM. (**D**) Effect of ^{VIC}oligo-4 on 48S formation and eIF4A crosslinking. The experiment was performed as in Figure 1C; as ^{VIC}oligo-4 reduced 48S formation, the volume of fraction 11 was adjusted to analyze an equivalent cpm. Arrows shows the direction of sedimentation.

that they placed at positions 27–28 of β-globin mRNA. We found that crosslinking efficiency of β-globin mRNA:probe was lower compared to SV and SFV mRNAs, probably because photoreactive 4-thio-U residues are not placed directly in the β-globin mRNA, but in the probe (Supplementary Figure S1A). Notably, probe:β-globin mRNA generated a pattern of protein crosslinking that included two bands of similar size to p48 (eIF4A) and p32 (Supplementary Figure S1B). In addition, this crosslinking revealed two specific bands (p42 and p80) that were not visible in SV DLP RNA samples. The identity of eIF4A was confirmed by denaturing IP, showing that eIF4A in the 48S complex can also contact AUG-downstream regions of cellular mRNA. The identity of p42 and p80 bands, and whether p80 is related to p75 band observed in complexes assembled with SV and SFV mRNAs, are unknown.

eIF4A acts on the ES6S region of the 40S subunit

Subsequent experiments were designed to identify the region of 40S where eIF4A contacts the DLP of SV mRNA. As a first approach, we compared the crosslinking patterns generated by SV DLP U1 mRNAs where DLP-AUG distance (d) were shortened to 19 nt or lengthened up to 37 nt. We previously found that DLP activity was strictly position dependent, showing a window of activity 25–50 nt downstream from the AUG (21). eIF4A crosslinking to $d = 19$ and $d = 37$ mRNAs was clearly reduced when compared to wild-type (WT) mRNA ($d = 28$), although $d = 37$ mRNA still retained 20–30% of WT levels (Figure 3A). It is important to note that the sequences flanking the DLP structure, as well the position of 4-thio-U are identical in these three mRNAs. Moreover, RNA folding programs predicted no alteration in the overall DLP structure in these mRNAs. Modeling of $d = 19$ mRNA in the 48S complex showed that the DLP structure is likely placed above ES6S region, probably near the mRNA entry channel (Figure 3B). Modeling of $d = 37$ mRNA, however, was compatible with DLP being placed on ES6S region, although stable interaction of photoreactive 4-thio-U residues with 18S rRNA was lost in both $d = 19$ and $d = 37$ mRNAs when compared to WT mRNA (Figure 3A and Supplementary Figure S2). These results show that eIF4A crosslinking depended on DLP position on the solvent side of the 40S subunit, suggesting that eIF4A may act on the ES6S region. It is important to note that $d = 19$ mRNA was unable to support translation in infected 3T3 cells, whereas DLP $d = 37$ mRNA showed a

Downloaded from https://academic.oup.com/nar/article-abstract/46/8/4176/4838059 by Spanish National Cancer Research Center user on 23 October 2018

translation similar or superior to WT mRNA (Figure 3C), suggesting that eIF4A crosslinking observed *in vitro* did not parallel translation of SV mRNA in infected cells.

Next, we analyzed the effect of a previously described synthetic oligonucleotide (^{VIC}oligo 4) (21) targeted to ES6S^{C} helix on eIF4A crosslinking (Figure 4A). We previously reported that binding of ^{VIC}oligo 4 to the 40S subunit inhibited translation of SV and SFV mRNA in infected cells (21), presumably by blocking the channel that extends between the ES6S^{A} and ES6S^{C-D} helices (Figure 4A). Pre-incubation of RRL with ^{VIC}oligo 4 inhibited translation of SV capsid mRNA that was detected by [^{35}S]Met labeling and autoradiography (Figure 4B), similar to that observed in infected cells (21). Furthermore, the observed reduction in 48S complex formation by ^{VIC}oligo 4 suggested that the ES6S region of 40S could be involved in SV mRNA attachment. Of note, pre-incubation with ^{VIC}oligo 4 drastically reduced the crosslinked eIF4A band detected in crude ribosomal fractions (P100) and 48S peak (Figure 4C and D), reinforcing the notion that ES6S is involved in eIF4A–mRNA contact.

Despite the high stability of the base of the DLP structure in SV and SFV mRNAs ($\Delta G^{\circ} = -20$–30 kcal.mol^{-1}), which exceeds the unwinding capability of eIF4A helicase (12,14), we wanted to test if a fraction of DLP stalled in the ES6S region could be effectively unwound by eIF4A. Thus, we compared the crosslinking of SV-DLP with 18S rRNA in the absence or in the presence of hippuristanol. We previously reported that the DLP contacts both the ES6S region and h16–h18 helices of 18S rRNA within the 48S complex, and that these contacts can be distinguished by an RNAse H assay using oligo 5.1 followed by separation in denaturing agarose gels (21). Inhibition of eIF4A activity increased the band intensity corresponding to mRNA crosslinked with the ES6S region (nt 680–830) of 18S rRNA, with a concomitant decrease in the band crosslinked with the h16–h18 region (nt 509–663) (Figure 5A). This can be interpreted as unwinding by eIF4A that releases a fraction of DLP structures from ES6S, leading to subsequent accumulation of DLP near the h16. To confirm this, we tested the effect of hippuristanol on toeprinting assays using a condensed version of SV 26S mRNA (see 'Materials and Methods' section). In the assembled 48S complex, primer extension by RT is typically arrested at 15–17 nt of mRNA, a result that has been used to roughly mark the leading edge of the 40S subunit into the scanning PIC (32–34). However, structural and biochemical data from synthetic mRNA threaded in the 40S binding cleft showed that the entry channel is ∼11 nt from the AUG of mRNA, showing that RT cannot penetrate completely in the entry channel (18,35,36). For 48S complexes assembled with SV DLP-capsid mRNA, in addition to the standard toeprints at 17–19 nt, we also detected minor arrests at 23–26 and 7–8 nt (Figure 5B). Toeprints at 23–26 nt may be suggestive of downstream interactions of mRNA with ES6S components of the 48S complex, whereas aberrant arrests at 7–8 nt have been interpreted as the result of incomplete mRNA threading into the 40S binding cleft (37). Importantly, toeprints at 23–26 nt were not detected in complexes assembled with SV ΔDLP capsid mRNA (Figure 5B), showing that these toeprints required DLP to stall in the ES6S region. Interestingly, hippuristanol treatment increased the proportion of toeprints at 23–26 nt and reduced the proportion of toeprints at 17–19 nt (Figure 5B), consistent with the notion that eIF4A indeed promotes the release of a fraction of unwound DLP from a region that was responsible for toeprints at 23–26 nt. This also implies that a substantial fraction of toeprints at 17–19 nt resulted from eIF4A-mediated release of DLP from downstream regions. We also observed that toeprints at 7–8 nt were also increased by hippuristanol treatment, suggesting that eIF4A activity is probably required for proper threading of mRNA *in vitro*.

To visualize eIF4A in 48S particles, we carried out immunogold labeling of eIF4A followed by EM using complexes assembled with SV-DLP U1 mRNA in RRL. Gradient fractions were first examined for the presence of associated eIFs, showing that the 48S peak contained eIF4A, eIF3 and eIF2 as expected (Figure 6A). Negative staining EM of peak 48S fractions also revealed the presence of contaminating 60S and isolated 40S subunits as described recently (38) (Supplementary Figure S3A). Next, the peak 48S fraction was incubated with an anti-eIF4A antibody, followed by incubation with 5 nm gold-coated protein A (GPA). Gold labels corresponding to eIF4A were detected in ∼5–10% of the total particles, whereas stochastically few labels were observed when primary antibodies were omitted, showing the specificity of the labeling (Supplementary Figure S3B). The low efficiency in the labeling could be reflecting a real occupancy of eIF4A on 40S subunits, or it could be attributable to the low accessibility of antibodies or/and GPA to the 40S subunit loaded with mRNA and eIFs. Assuming that labels are spaced up to 17 nm from the antibody-binding site (39), the gold would be the center of a 17 nm-radius circle containing the antigen. We selected and analyzed 20 particles whose projections were identified, showing that eIF4A labels were concentrated in the solvent side of 40S. In about half of these particles, gold labels were located between eIF3 and the 40S body (class I), whereas the rest of the particles had gold near the feet (30%, class II) or the beak of the 40S head (15%, class III). Interestingly, we found some particles where two gold labels corresponding to eIF4A were detected (Figure 6B). To complement this result, we mapped the position of gold bound to SV DLP mRNA on the 48S complex. For this, we designed a 5′-biotinylated RNA oligo targeted to 25–37 nt downstream of the AUG of SV ΔDLP U1 mRNA that mimics the natural DLP structure (Supplementary Figure S3C). We roughly estimate that the streptavidin-nanogold particle bound to the biotinylated oligo is extended 6–10 nm from the 5′ end of the oligo, although in this case an accurate measurement of the spacing was impossible. Analysis of the peak 48S fraction revealed labels in ∼10% of total particles concentrated on the solvent side of the 40S subunit near the feet, although we also detected some particles with labels near the classical mRNA entry channel, or even below the beak of the 40S subunit (Figure 6C). In both types of labeling, we also detected additional particle densities on the solvent side that could be attributable to antibody and/or the presence of eIF4F in the complex.

Downloaded from https://academic.oup.com/nar/article-abstract/46/8/4176/4838059 by Spanish National Cancer Research Center user on 23 October 2018

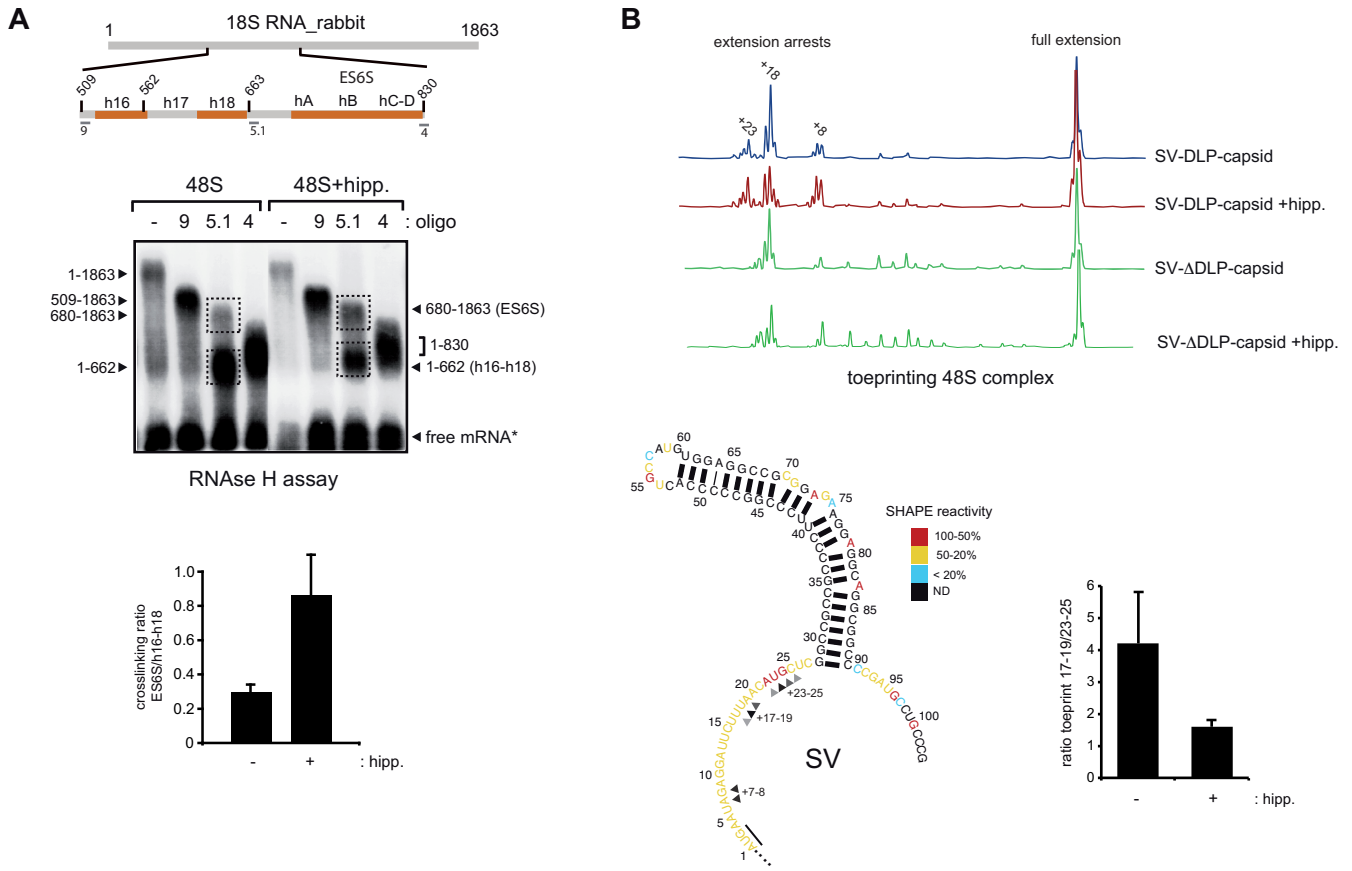

Figure 5. eIF4A activity within the 48S complex. (**A**) RNase H-mapping of RNA–RNA interactions between SV-DLP U1 and 18S rRNA. The analysis was carried out in the absence or presence of 1 μM hippuristanol, with identification of the resulting RNA fragments indicated. For clarity, a schematic diagram of the ES6S and h16–18 regions of rabbit 18S rRNA with the primers used for RNase H digestion is shown. The use of oligos 4 and 9 limited the region of 18S rRNA (509–830) where the crosslinkings concentrated. Bands corresponding to crosslinking of SV DLP U1 mRNA with the ES6S region (680–1863) and h16-h18 helices (1–662) were quantified by densitometry and expressed as a ratio. Data are the mean ± SEM from four independent experiments. (**B**) Effect of eIF4A inhibition on 48S toeprinting generated by SV-DLP U1 and SV-ΔDLP U1 mRNAs. Assays were carried out in the absence of presence of 1 μM of hippuristanol; positions of resulting primer extensions are annotated with respect to the A (+1) position of AUG, and they have been assigned with a precision of ±1 nt. The bottom shows a 2D structural model of the first 100 nt of 26S mRNA, showing the secondary structure derived from SHAPE analysis (21). Reactivity to SHAPE reagent (NMIA) is higher for unpaired nucleotides (red) and low for those involved in pairings (black). Stops corresponding to toeprints are marked with arrowheads. Quantification of toeprint ratios (17–19/23–25) in absence or presence of hippuristanol is shown from three independent experiments; data are the mean ± SEM.

eIF4A activity is detrimental to translation of SV mRNA in infected cells

Since DLP integrity is essential for eIF2-independent translation of SV mRNA in infected cells (21,24), it was thought that eIF4F-mediated unwinding of SV DLP RNA could be detrimental to viral mRNA translation in mammalian cells. Previous studies have reported that translation of SV 26S mRNA in infected cells shows low dependence on eIF4F activity (40). Moreover, exclusion of some eIFs (eIF2 and 4F) from viral factories has been reported in infected cells. To confirm this, we analyzed the distribution of eIF4A in SFV-infected cells by means of IF, showing a dramatic exclusion of eIF4A from viral factories with active translation of viral mRNAs (Figure 7A). Given this exclusion, the eIF4A activity outside the viral factories is expected to have a minimal impact on DLP-dependent translation in infected cells, which prompted us to test the effect of forced eIF4A expression within viral factories by using recombinant SV that encode human eIF4A (see 'Materials and Methods' section). As is shown in Figure 7B, accumulation of recombinant eIF4A co-localized with viral capsid proteins, representative of viral factories (41). Viruses expressing eIF4A showed a 60–70% reduction in the synthesis of viral proteins, indicating that ectopic expression of eIF4A in viral factories interfered with translation of SV 26S mRNA.

DISCUSSION

During adaptation to the host, viruses often find simple solutions to better translate their mRNAs in a manner less dependent on eIFs. In some cases, these viral tricks have been used to infer the function of eIFs in canonical initiation, a task that has also required the analysis of viral translation outside of infected cells (42). For SV and SFV 26S mRNA, the acquisition of a stable DLP structure in mRNA emerged as a solution to locate the start AUG when eIF2 becomes phosphorylated in infected cells (23). The situation is clearly

Downloaded from https://academic.oup.com/nar/article-abstract/46/8/4176/4838059 by Spanish National Cancer Research Center user on 23 October 2018

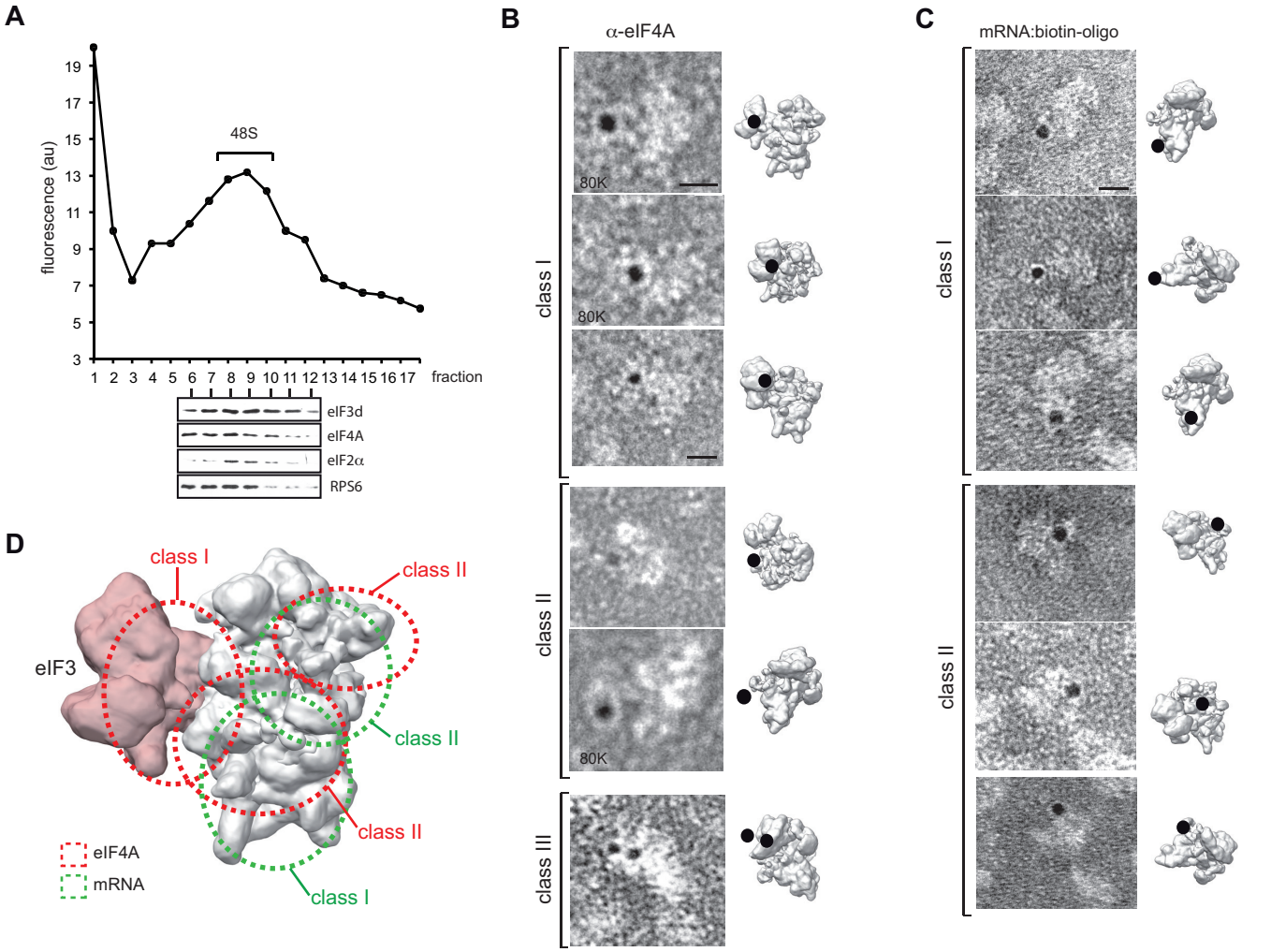

Figure 6. EM localization of eIF4A and mRNA in the 48S complex. (**A**) Analysis of the eIF composition of 48S complexes assembled with SV-DLP U1 mRNA. A small amount of fluorescein-labeled SV-DLP U1 mRNA was included in the reaction to identify the fraction corresponding to 48S peaks. Fractions 6–12 were precipitated in acetone–chloroform and analyzed by western blot using the indicated antibodies. Fractions 8–10 were pooled and subjected to immuno-EM using an α-eIF4A antibody followed by incubation with 5 nm GPA. (**B**) Gallery of most abundant views grouped into three classes. Photographs were taken at 60K (except otherwise indicated) and the corresponding projections on the 43S model (EM-5658) are shown Scale bar corresponds to 10 nm. (**C**) Gallery of most abundant views of the 48S complex assembled with SV ΔDLP mRNA bound to a 5′-biotinylated antisense RNA oligo (see Supplementary Figure S3C for details). In this case, the samples were incubated with streptavidin-5 nm gold as described in the 'Materials and Methods' section. (**D**) Superposition of all labels for eIF4A (red) and for mRNA (green), showing the most likely placement areas.

different in RRL programmed with SV mRNA, since these extracts contain high concentrations of ribosomes and fully active eIFs (43). Here, using RRL to assemble 48S complexes with SFV and SV mRNAs free of any viral interference, we were able to detect for the first time the interaction of eIF4A within the 48S complex with nucleotides located downstream from the start AUG. This interaction was only detected when the crosslinkable residues were placed flanking the DLP structure of the mRNA, suggesting that the stability of the DLP base was great enough to jam a fraction of eIF4A molecules on the mRNA. This conclusion is consistent with the limits on unwinding activity previously estimated for eIF4A ($\Delta G^{\circ} = -20$–30 kcal.mol^{-1}) by using helicase assays *in vitro* with RNA duplex substrates (12,44). The binding of eIF4A to single stranded flanking the DLP structure agrees well with previous reports showing a strong preference of yeast eIF4F for a single stranded region to unwind duplex RNAs (45), although a similar preference was not observed in mammalian eIF4F (44,46). Whether eIF4A enters as free molecule or as part of eIF4F complex in 48S complex assembled with SV and SFV mRNAs is unknown. Nonetheless, in RRL programmed with SV mRNA we found considerable unwinding activity by eIF4A on SV DLP-ES6S, an interaction that was attenuated by hippuristanol treatment, suggesting that eIF4A probably releases a fraction of mRNA molecules from the ES6S region, leading to the appearance of new contacts with upper regions of rRNA (h16 and h18) in the 48S complex. This detrimental effect that eIF4A has on DLP stability and viral mRNA translation offers a convincing causative explanation for the exclusion of eIF4F from viral factories observed in infected cells, and illustrates an example of how a game of RNA stability played between the virus and host resulted in translational adaptation by the former. At this time, it is not clear

Downloaded from https://academic.oup.com/nar/article-abstract/46/8/4176/4838059 by Spanish National Cancer Research Center user on 23 October 2018

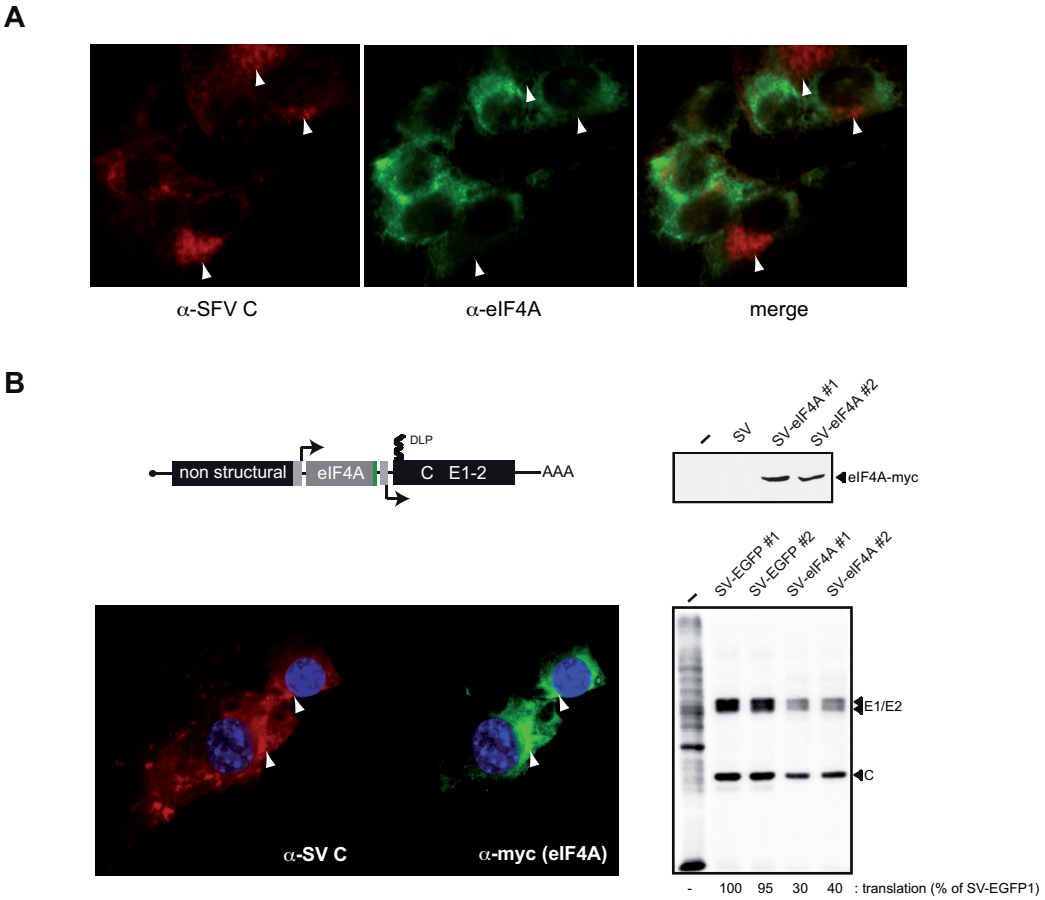

Figure 7. Ectopic expression of eIF4A in viral factories reduced SV mRNA translation. (**A**) Exclusion of eIF4A from SFV viral factories. IF of eIF4A in mock and SFV-infected cells, with SFV C protein stained in red and eIF4A in green. Note the exclusion of eIF4A from viral factories as revealed by C protein staining (arrowheads). About 75% of analyzed cells showed this pattern, and a representative field is shown. (**B**) Schematic representation of recombinant SV expressing human eIF4A-myc. Cells were infected with two independent SV-eIF4A clones and analyzed by western blot against myc epitope (right upper panel), by IF against SV C and myc epitopes (left lower), and by metabolic labeling with [^{35}S]-Met. The position of viral protein bands is indicated; in all cases, samples were analyzed at 6 hpi, with two SV clones expressing EGFP used as controls.

whether the lack of eIF4A in viral factories involves active removal of eIF4F or simply its exclusion from the 40S-eIF3 complexes that are concentrated within viral factories (41), so further studies are required to clarify this point.

The detection of toeprints at nt 23–25, whose relative intensity increased upon hippuristanol treatment, reinforces the idea that eIF4A is acting on the ES6S region of 40S, converting the incoming mRNA into a single-stranded form during its approach to the entry channel to give the canonical toeprints at 17–19 nt. Interestingly, recent analysis of initiation complex-specific ribosome footprints in yeast has revealed that, in addition to the main +16 nt protection, mRNA is also protected at +25 nt from the AUG, a finding that nicely agrees with data presented here if we assume that mRNA is threaded into the ES6S region before reaching the classical mRNA entry channel (47). Thus, the interaction of flanking nucleotides of the DLP structure with the ES6S region that we reported recently could easily explain the RT stops at 23–25 nt found here (21). The crosslinking of SV and SFV mRNAs with both exposed (helices A and B) and inner ES6S segments (helix C and D) suggests that these mRNAs could be penetrating the ES6S region (21,22), a notion that is further supported by the inhibitory effect of with ^{VIC}oligo 4 on translation of SV 26S mRNA observed in cultured cells (21) and in RRL shown here. The results using ^{VIC}oligo 4, or when moving the DLP structure upstream by 9 nt (equivalent to 40 Å) further support the notion that the eIF4A helicase, probably as part of the eIF4F complex, is placed on (or near) the ES6S region of the 40S subunit during scanning. This location agrees well with data showing that the middle domain of eIF4G (eIF4G-MD) contacted with ES6S^{E} and ES6S^{B} projections of 40S when initiation complexes were assembled in the presence of viral mRNA (48), and by a recent report showing that mRNA attachment occurs on the solvent side of 40S through a chain of interactions that involves eIF4F and eIF3 (3). Our data also support short-range activity for eIF4A since its interaction with the base of the DLP was dependent on DLP-AUG$_i$ spacing. Perhaps most eIF4A molecules in 43S–mRNA complexes are immobilized via interaction with eIF4G, although the low (but still detectable) level of crosslinking of eIF4A to the base of DLP $d = 19$ is compatible with a small fraction of eIF4A acting in a diffusible manner. Alternatively, it is possible that two

Downloaded from https://academic.oup.com/nar/article-abstract/46/8/4176/4838059 by Spanish National Cancer Research Center user on 23 October 2018

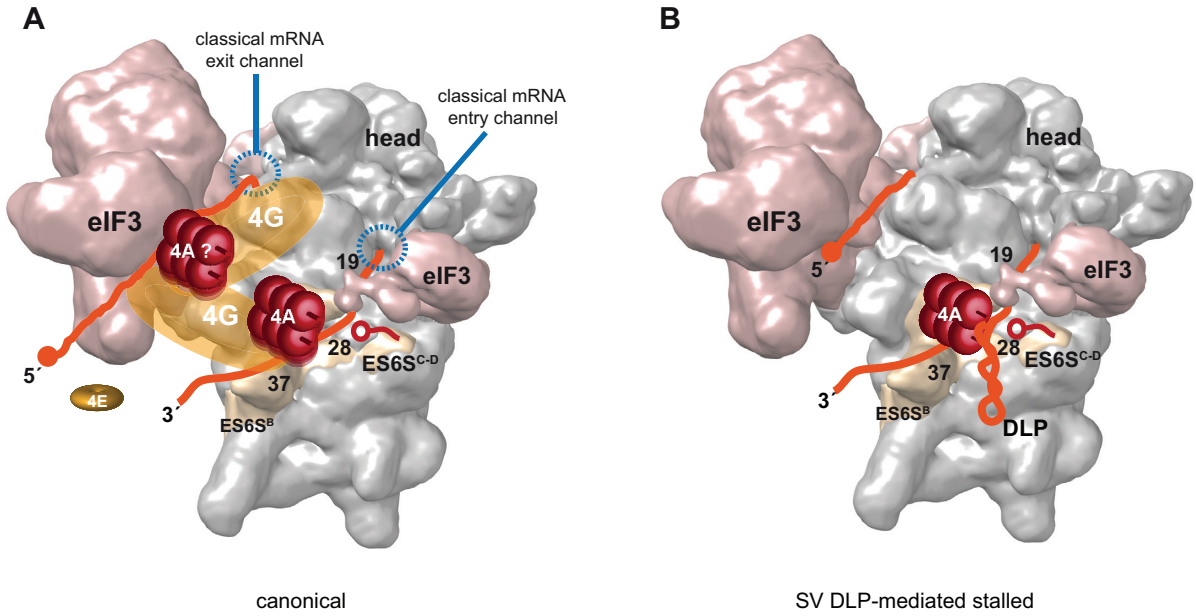

Figure 8. Model of PIC scanning. (**A**) Canonical model of PIC scanning with eIF4F complex placed on ES6S region of 40S subunit (EM-5658) (19), interacting with both 3′and 5′regions of mRNA (orange). The scaffolding eIF4G factor is in yellow, interacting with both ES6S (48) and eIF3 as reported before (49,50). In this model two molecules of eIF4A (red rollers) are placed on eIF4G according to previous data (13,15). The 4E subunit of eIF4F (eIF4E) is dissociated from the cap structure upon 48S complex formation as suggested recently (3). (**B**) SV DLP-mediated stalled PIC showing one eIF4A molecule jammed by DLP structure on ES6S region. The rest of factors and details were omitted for simplicity. The position of ^{VIC}oligo-4 is also shown (red).

molecules of eIF4A could be acting within the 48S complex in a coordinated manner, acting one of them in a diffusible manner (Figure 8A) (15). The presence of two gold labels found in some 48S particles when staining for eIF4A by EM could support this possibility.

Taken together, data presented here supports a model where the eIF4F complex is working at the leading edge of the scanning PIC, rather than acting as a simple clamp to prevent backsliding as suggested previously (16). Nonetheless, the extended topology that eIF4G presumably adopts could promote simultaneous binding of eIF4F to the 5′ and 3′ ends of mRNA, bringing the two ends of mRNA near the body of 40S in a way that could allow an eIF4A/4B tandem working on the front (3′-pulling) and back (5′-pushing) in a coupled manner (15,49,50).

SUPPLEMENTARY DATA

Supplementary Data are available at NAR Online.

ACKNOWLEDGEMENTS

We are indebted to Jerry Pelletier (McGill University) for providing us with hippuristanol. We also thank the Genomics Facility at the López Neira Institute (Granada, Spain) for efficient analysis of toeprinting products, and the Electron Microscopy facility of the CBMSO for negative staining EM.

FUNDING

Ministerio de Ciencia e Innovación [BFU2013-4005R]. Funding for open access charge: Spanish Minister of Science National Grant [BFU1013-4005R].

Conflict of interest statement. None declared.

REFERENCES

1. Hinnebusch,A.G. (2011) Molecular mechanism of scanning and start codon selection in eukaryotes. *Microbiol. Mol. Biol. Rev.*, **75**, 434–467.
2. Jackson,R.J., Hellen,C.U. and Pestova,T.V. (2010) The mechanism of eukaryotic translation initiation and principles of its regulation. *Nat. Rev. Mol. Cell Biol.*, **11**, 113–127.
3. Kumar,P., Hellen,C.U. and Pestova,T.V. (2016) Toward the mechanism of eIF4F-mediated ribosomal attachment to mammalian capped mRNAs. *Genes Dev.*, **30**, 1573–1588.
4. Aitken,C.E., Beznoskova,P., Vlckova,V., Chiu,W.L., Zhou,F., Valasek,L.S., Hinnebusch,A.G. and Lorsch,J.R. (2016) Eukaryotic translation initiation factor 3 plays distinct roles at the mRNA entry and exit channels of the ribosomal preinitiation complex. *Elife*, **5**, e20934.
5. Svitkin,Y.V., Pause,A., Haghighat,A., Pyronnet,S., Witherell,G., Belsham,G.J. and Sonenberg,N. (2001) The requirement for eukaryotic initiation factor 4A (eIF4A) in translation is in direct proportion to the degree of mRNA 5′ secondary structure. *RNA*, **7**, 382–394.
6. Pestova,T.V. and Kolupaeva,V.G. (2002) The roles of individual eukaryotic translation initiation factors in ribosomal scanning and initiation codon selection. *Genes Dev.*, **16**, 2906–2922.
7. Pelletier,J. and Sonenberg,N. (1985) Insertion mutagenesis to increase secondary structure within the 5′ noncoding region of a eukaryotic mRNA reduces translational efficiency. *Cell*, **40**, 515–526.
8. Kozak,M. (1989) Circumstances and mechanisms of inhibition of translation by secondary structure in eucaryotic mRNAs. *Mol. Cell. Biol.*, **9**, 5134–5142.
9. Babendure,J.R., Babendure,J.L., Ding,J.H. and Tsien,R.Y. (2006) Control of mammalian translation by mRNA structure near caps. *RNA*, **12**, 851–861.
10. Parsyan,A., Svitkin,Y., Shahbazian,D., Gkogkas,C., Lasko,P., Merrick,W.C. and Sonenberg,N. (2011) mRNA helicases: the tacticians of translational control. *Nat. Rev. Mol. Cell Biol.*, **12**, 235–245.

Downloaded from https://academic.oup.com/nar/article-abstract/46/8/4176/4838059 by Spanish National Cancer Research Center user on 23 October 2018

11. Ray,B.K., Lawson,T.G., Kramer,J.C., Cladaras,M.H., Grifo,J.A., Abramson,R.D., Merrick,W.C. and Thach,R.E. (1985) ATP-dependent unwinding of messenger RNA structure by eukaryotic initiation factors. *J. Biol. Chem.*, **260**, 7651–7658.
12. Rogers,G.W. Jr, Richter,N.J. and Merrick,W.C. (1999) Biochemical and kinetic characterization of the RNA helicase activity of eukaryotic initiation factor 4A. *J. Biol. Chem.*, **274**, 12236–12244.
13. Nielsen,K.H., Behrens,M.A., He,Y., Oliveira,C.L., Jensen,L.S., Hoffmann,S.V., Pedersen,J.S. and Andersen,G.R. (2011) Synergistic activation of eIF4A by eIF4B and eIF4G. *Nucleic Acids Res.*, **39**, 2678–2689.
14. Garcia-Garcia,C., Frieda,K.L., Feoktistova,K., Fraser,C.S. and Block,S.M. (2015) RNA BIOCHEMISTRY. Factor-dependent processivity in human eIF4A DEAD-box helicase. *Science*, **348**, 1486–1488.
15. Marintchev,A., Edmonds,K.A., Marintcheva,B., Hendrickson,E., Oberer,M., Suzuki,C., Herdy,B., Sonenberg,N. and Wagner,G. (2009) Topology and regulation of the human eIF4A/4G/4H helicase complex in translation initiation. *Cell*, **136**, 447–460.
16. Spirin,A.S. (2009) How does a scanning ribosomal particle move along the 5′-untranslated region of eukaryotic mRNA? Brownian Ratchet model. *Biochemistry*, **48**, 10688–10692.
17. des Georges,A., Dhote,V., Kuhn,L., Hellen,C.U., Pestova,T.V., Frank,J. and Hashem,Y. (2015) Structure of mammalian eIF3 in the context of the 43S preinitiation complex. *Nature*, **525**, 491–495.
18. Lomakin,I.B. and Steitz,T.A. (2013) The initiation of mammalian protein synthesis and mRNA scanning mechanism. *Nature*, **500**, 307–311.
19. Hashem,Y., des Georges,A., Dhote,V., Langlois,R., Liao,H.Y., Grassucci,R.A., Hellen,C.U., Pestova,T.V. and Frank,J. (2013) Structure of the mammalian ribosomal 43S preinitiation complex bound to the scanning factor DHX29. *Cell*, **153**, 1108–1119.
20. Erzberger,J.P., Stengel,F., Pellarin,R., Zhang,S., Schaefer,T., Aylett,C.H., Cimermancic,P., Boehringer,D., Sali,A., Aebersold,R. *et al.* (2014) Molecular architecture of the 40SeIF1eIF3 translation initiation complex. *Cell*, **158**, 1123–1135.
21. Toribio,R., Diaz-Lopez,I., Boskovic,J. and Ventoso,I. (2016) An RNA trapping mechanism in Alphavirus mRNA promotes ribosome stalling and translation initiation. *Nucleic Acids Res.*, **44**, 4368–4380.
22. Toribio,R., Diaz-Lopez,I. and Ventoso,I. (2016) New insights into the topology of the scanning ribosome during translation initiation: lessons from viruses. *RNA Biol.*, **13**, 1223–1227.
23. Ventoso,I. (2012) Adaptive changes in alphavirus mRNA translation allowed colonization of vertebrate hosts. *J. Virol.*, **86**, 9484–9494.
24. Ventoso,I., Sanz,M.A., Molina,S., Berlanga,J.J., Carrasco,L. and Esteban,M. (2006) Translational resistance of late alphavirus mRNA to eIF2alpha phosphorylation: a strategy to overcome the antiviral effect of protein kinase PKR. *Genes Dev.*, **20**, 87–100.
25. Sanz,M.A., Gonzalez Almela,E. and Carrasco,L. (2017) Translation of sindbis subgenomic mRNA is independent of eIF2, eIF2A and eIF2D. *Sci. Rep.*, **7**, 43876.
26. Skabkin,M.A., Skabkina,O.V., Dhote,V., Komar,A.A., Hellen,C.U. and Pestova,T.V. (2010) Activities of ligatin and MCT-1/DENR in eukaryotic translation initiation and ribosomal recycling. *Genes Dev.*, **24**, 1787–1801.
27. Lee,A.S., Kranzusch,P.J. and Cate,J.H. (2015) eIF3 targets cell-proliferation messenger RNAs for translational activation or repression. *Nature*, **522**, 111–114.
28. Dmitriev,S.E., Pisarev,A.V., Rubtsova,M.P., Dunaevsky,Y.E. and Shatsky,I.N. (2003) Conversion of 48S translation preinitiation complexes into 80S initiation complexes as revealed by toeprinting. *FEBS Lett.*, **533**, 99–104.
29. Wilkinson,K.A., Merino,E.J. and Weeks,K.M. (2006) Selective 2′-hydroxyl acylation analyzed by primer extension (SHAPE): quantitative RNA structure analysis at single nucleotide resolution. *Nat. Protoc.*, **1**, 1610–1616.
30. Schneider-Poetsch,T., Ju,J., Eyler,D.E., Dang,Y., Bhat,S., Merrick,W.C., Green,R., Shen,B. and Liu,J.O. (2010) Inhibition of eukaryotic translation elongation by cycloheximide and lactimidomycin. *Nat. Chem. Biol.*, **6**, 209–217.
31. Bordeleau,M.E., Mori,A., Oberer,M., Lindqvist,L., Chard,L.S., Higa,T., Belsham,G.J., Wagner,G., Tanaka,J. and Pelletier,J. (2006) Functional characterization of IRESes by an inhibitor of the RNA helicase eIF4A. *Nat. Chem. Biol.*, **2**, 213–220.
32. Pisarev,A.V., Unbehaun,A., Hellen,C.U. and Pestova,T.V. (2007) Assembly and analysis of eukaryotic translation initiation complexes. *Methods Enzymol.*, **430**, 147–177.
33. Hartz,D., McPheeters,D.S., Traut,R. and Gold,L. (1988) Extension inhibition analysis of translation initiation complexes. *Methods Enzymol.*, **164**, 419–425.
34. Anthony,D.D. and Merrick,W.C. (1992) Analysis of 40 S and 80 S complexes with mRNA as measured by sucrose density gradients and primer extension inhibition. *J. Biol. Chem.*, **267**, 1554–1562.
35. Pisarev,A.V., Kolupaeva,V.G., Yusupov,M.M., Hellen,C.U. and Pestova,T.V. (2008) Ribosomal position and contacts of mRNA in eukaryotic translation initiation complexes. *EMBO J.*, **27**, 1609–1621.
36. Martin,F., Menetret,J.F., Simonetti,A., Myasnikov,A.G., Vicens,Q., Prongidi-Fix,L., Natchiar,S.K., Klaholz,B.P. and Eriani,G. (2016) Ribosomal 18S rRNA base pairs with mRNA during eukaryotic translation initiation. *Nat. Commun.*, **7**, 12622.
37. Abaeva,I.S., Marintchev,A., Pisareva,V.P., Hellen,C.U. and Pestova,T.V. (2011) Bypassing of stems versus linear base-by-base inspection of mammalian mRNAs during ribosomal scanning. *EMBO J.*, **30**, 115–129.
38. Simonetti,A., Brito Querido,J., Myasnikov,A.G., Mancera-Martinez,E., Renaud,A., Kuhn,L. and Hashem,Y. (2016) eIF3 peripheral subunits rearrangement after mRNA binding and start-codon recognition. *Mol. Cell*, **63**, 206–217.
39. Wolf,E., Kastner,B., Deckert,J., Merz,C., Stark,H. and Luhrmann,R. (2009) Exon, intron and splice site locations in the spliceosomal B complex. *EMBO J.*, **28**, 2283–2292.
40. Castello,A., Sanz,M.A., Molina,S. and Carrasco,L. (2006) Translation of Sindbis virus 26S mRNA does not require intact eukariotic initiation factor 4G. *J. Mol. Biol.*, **355**, 942–956.
41. Garcia-Moreno,M., Sanz,M.A., Pelletier,J. and Carrasco,L. (2013) Requirements for eIF4A and eIF2 during translation of Sindbis virus subgenomic mRNA in vertebrate and invertebrate host cells. *Cell Microbiol.*, **15**, 823–840.
42. Walsh,D., Mathews,M.B. and Mohr,I. (2013) Tinkering with translation: protein synthesis in virus-infected cells. *Cold Spring Harb. Perspect. Biol.*, **5**, a012351.
43. Jackson,R.J. and Hunt,T. (1983) Preparation and use of nuclease-treated rabbit reticulocyte lysates for the translation of eukaryotic messenger RNA. *Methods Enzymol.*, **96**, 50–74.
44. Rozen,F., Edery,I., Meerovitch,K., Dever,T.E., Merrick,W.C. and Sonenberg,N. (1990) Bidirectional RNA helicase activity of eucaryotic translation initiation factors 4A and 4F. *Mol. Cell. Biol.*, **10**, 1134–1144.
45. Rajagopal,V., Park,E.H., Hinnebusch,A.G. and Lorsch,J.R. (2012) Specific domains in yeast translation initiation factor eIF4G strongly bias RNA unwinding activity of the eIF4F complex toward duplexes with 5′-overhangs. *J. Biol. Chem.*, **287**, 20301–20312.
46. Rogers,G.W. Jr, Lima,W.F. and Merrick,W.C. (2001) Further characterization of the helicase activity of eIF4A. Substrate specificity. *J. Biol. Chem.*, **276**, 12598–12608.
47. Archer,S.K., Shirokikh,N.E., Beilharz,T.H. and Preiss,T. (2016) Dynamics of ribosome scanning and recycling revealed by translation complex profiling. *Nature*, **535**, 570–574.
48. Yu,Y., Abaeva,I.S., Marintchev,A., Pestova,T.V. and Hellen,C.U. (2011) Common conformational changes induced in type 2 picornavirus IRESs by cognate trans-acting factors. *Nucleic Acids Res.*, **39**, 4851–4865.
49. LeFebvre,A.K., Korneeva,N.L., Trutschl,M., Cvek,U., Duzan,R.D., Bradley,C.A., Hershey,J.W. and Rhoads,R.E. (2006) Translation initiation factor eIF4G-1 binds to eIF3 through the eIF3e subunit. *J. Biol. Chem.*, **281**, 22917–22932.
50. Villa,N., Do,A., Hershey,J.W. and Fraser,C.S. (2013) Human eukaryotic initiation factor 4G (eIF4G) protein binds to eIF3c, -d, and -e to promote mRNA recruitment to the ribosome. *J. Biol. Chem.*, **288**, 32932–32940.

Downloaded from https://academic.oup.com/nar/article-abstract/46/8/4176/4838059 by Spanish National Cancer Research Center user on 23 October 2018